This article has been accepted for publication in a future issue of this journal, but has not been fully edited. Content may change prior to final publication. Citation information: DOI 10.1109/TIA.2018.2820640, IEEE Transactions on Industry Applications

Single-Phase Soft-Switched AC-AC Matrix Converter with Power Controller for Bidirectional Inductive Power Transfer Systems

Masood Moghaddami, *Student Member, IEEE,* and Arif I. Sarwat, *Senior Member, IEEE*

***Abstract*—A direct soft-switched single-phase AC-AC matrix converter for bidirectional inductive power transfer (IPT) systems is proposed. Quantum energy injection/regeneration principle is used to design a simplified digital power controller that enables the converter to establish bidirectional power transfer between the IPT system and single-phase AC mains at a desired power level. The simplified controller can be implemented using basic logic circuit components, without the need for DSP/FPGA platforms, thereby reducing the complexity and the implementation cost. The converter benefits from resonance frequency tracking capability for the synchronization of switching operations of the converter with the resonant current which makes it ideal for dynamic IPT systems. Also, it benefits from soft-switching operations to achieve an enhanced efficiency and low electromagnetic interference (EMI). The converter is specifically suitable for establishing grid-to-vehicle (G2V) and vehicle-to-grid (V2G) connections through inductive electric vehicle charging/discharging systems. The proposed converter is analyzed theoretically, is simulated in MATLAB/Simulink, and finally is verified experimentally at low power on a case study IPT system. The results show that the proposed matrix converter can effectively establish bidirectional power transfer at different power levels with soft-switching operation and resonance frequency tracking capability.**

***Index Terms*—AC-AC converter, bidirectional inductive power transfer, direct matrix converter, power control.**

I. Introduction

INDUCTIVE power transfer (IPT) is a new technology that enables contactless electric vehicle (EV) charging, offering more convenience to the use of EVs. Therefore, it can contribute to the adoption of EVs in transportation systems. Inductive EV charging technology is branched into two major group: static charging [1]–[3] and dynamic charging [4]–[8]. In static inductive charging systems, EVs are charged while they are parked in a parking spot, while in dynamic inductive charging systems EVs can be charged while they are moving. Also, this emerging technology can be used to integrate EVs with power grid by making bidirectional grid-to-vehicle (G2V) and vehicle-to-grid (V2G) connections [9]–[12]. Specifically, V2G connections are of a great interest for the future power grids as they can be used to support the power grid in extreme conditions, such as black-outs [13], [14]. In Fig. 1, a typical bidirectional IPT system consisting of magnetic coupling structures, compensation circuits, and primary and secondary bidirectional converters.

This work was supported by the National Science Foundation under grant number 1541108 and FIU Graduate School Dissertation Year Fellowship.

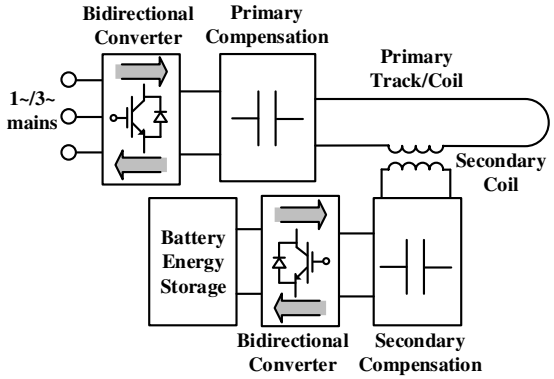

Fig. 1. The structure of a bidirectional IPT system.

Bidirectional IPT systems have been studied in [12], [15], [16]. The magnetic structures in IPT systems are inherently capable of transferring power in either direction. However, in order to enable bidirectional power transfer in IPT systems, the use of bidirectional power converters is essential. Specifically, a bidirectional AC-AC converter is essential in the primary side, as an interface between AC mains and the IPT system. Conventionally, two-stage AC-AC converters are used for IPT systems including H-bridge converters [16], current source converters [12], [15], z-source inverters [17], multilevel inverters [18]. However, in recent years there has been an increasing interest in matrix converters (MCs) [19]–[22]. MCs are used to directly convert AC mains inputs to a high-frequency AC (HFAC) output without any intermediate conversion stage. In MCs, the bulky energy storage elements are eliminated and thereby, they have high power density and are more reliable. Specifically, three-phase to single-phase and single-phase to single-phase matrix converters are of great interest in IPT systems. These types of converters have been successfully employed with a reduced number of elements and improved efficiency [20], [21]. Since MCs are inherently bidirectional they can be used to regenerate power from an IPT system back into the source and as a result, they can be used for inductive EV charging/discharging applications, where G2V and V2G connections can be established. Resonant MCs have been of great interest in many applications. In [22], a single-phase AC-AC resonant converter with soft-switching operation sliding-mode control is introduced.

In [19], a single-phase MC based on a modulation technique for bidirectional IPT systems is proposed. The converter

This article has been accepted for publication in a future issue of this journal, but has not been fully edited. Content may change prior to final publication. Citation information: DOI 10.1109/TIA.2018.2820640, IEEE Transactions on Industry Applications

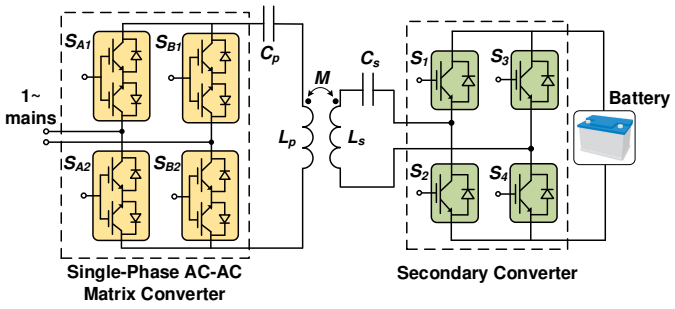

Fig. 2. Series-compensated bidirectional IPT system with a single-phase AC-AC MC as the primary converter and a conventional H-bridge converter as the secondary converter.

enables attenuation of the harmonic distortions in the grid current. However, the converter is hard-switched, which leads to a lower efficiency and reliability and requires complex commutation techniques. Quantum resonant converters which are introduced in 1989 [23] has found an increasing interest for IPT systems. In [20], a half-bridge single-phase quantum MC comprised of two bidirectional switches is proposed. Due to the reduced number of switches used in the converter, it can inject energy in half of the resonant current half-cycles and therefore, the maximum power transfer is limited.

The resonance frequency in an IPT system can slightly deviate from its nominal point due to changes in operating conditions. The deviation of switching operations from resonance point can dramatically affect the performance of the system. Therefore, constant switching adjustment to the resonance frequency variations is essential to ensure high power transfer efficiency in the system. The resonance frequency tracking capability of the controller enables synchronization of the switching operation of the converters with the resonant current to achieve maximum power transfer with high efficiency [24]–[27].

In this paper, a soft-switched single-phase direct AC-AC matrix converter with a power transfer controller for bidirectional IPT systems which is developed based on our previous work in [28] is presented. With regular 120V/240V single-phase supply, the power transfer levels that can be obtained include standard power levels as defined by SAE J2954 for light-duty EVs [29]. The power transfer regulation is achieved based on energy injection/regeneration principle. The proposed controller benefits from resonance frequency tracking capability to constantly synchronize the switching operations of the converter with the resonant current. Also, it achieves zero-current switching (ZCS), which in turn eliminates the need for conventional multi-stage commutation techniques. The power controller is designed and implemented based on a digital circuit composed of basic logic level components without the use of FPGA/DSP solutions, thereby making it a low-cost solution. Theoretical and simulation analyses and experimental validations of the proposed direct AC-AC matrix converter along with its controller are presented in detail.

II. Power Transfer Controller for Direct Single-Phase AC-AC Converter

In Fig. 2, a series-series compensated bidirectional IPT system with a direct single-phase AC-AC MC as the primary converter and an H-bridge converter as the secondary converter is shown. The IPT system is represented by primary and secondary self-inductances L_p and L_s, primary and secondary compensation capacitors C_p and C_s. The primary converter is comprised of four bidirectional switches (S_{A1}, S_{A2}, S_{B1}, S_{B2}).

A power controller is designed for the AC-AC converter that enables power transfer at the desired level by tuning the energy injection/regeneration rate in the IPT system. The controller takes resonant current (i_r) and AC supply voltage (v_{ac}) as feedbacks and generates four switching signals for the AC-AC converter. The controller is designed to enable soft-switching operations at the resonant current zero-crossing points. In other words, each operation mode starts and ends at current zero-crossing points, forming a half-cycle. The zero-current switching (ZCS) significantly reduces the complexity of commutation usually required in matrix converters and eliminates the need for conventional four stage commutation techniques. The controller is composed of two main sections: switching logic and energy injection/regeneration frequency divider. The quantum energy injection/regeneration principle and the design methodology for each section of the controller are described as follows.

A. Quantum Energy Injection/Regeneration Principle for Power Transfer Control

Loosely-coupled IPT systems operate based on resonant magnetic induction to enable power transmission through large air gaps. In such systems, the inductance of the coils and compensation capacitors form LC tanks (in both primary and secondary sides) in which a buffer energy is stored. The power transfer level in an IPT system can be regulated by controlling the buffer energy stored in the LC tanks. Quantum energy injection/regeneration to/from LC tank is a technique which can be used to control the buffer energy and consequently the power transfer level of the IPT system. This control method can be applied to the single-phase AC-AC matrix converter which is shown as a primary converter in Fig. 2. Based on this method energy can be transferred from/to the single-phase power source to/from the primary LC tank in the form of quantum energy pulses which exactly correspond to the resonant current half-cycles. In the half-cycles in which energy transfer is not desired, the IPT system enters a freewheeling mode in which the resonant current is freewheeled in order to continue its natural oscillation.

In Fig. 3, the application of this technique on the single-phase converter is conceptually shown at different operating conditions. This figure shows the concept plots of resonant current, energy injection or regeneration signal, grid current and grid voltage where (a), (b) represent forward power transfer mode with positive and negative grid voltages, and (c), (d) represent reverse power transfer mode with positive and negative grid voltages. As it can be seen, in forward power

This article has been accepted for publication in a future issue of this journal, but has not been fully edited. Content may change prior to final publication. Citation information: DOI 10.1109/TIA.2018.2820640, IEEE Transactions on Industry Applications

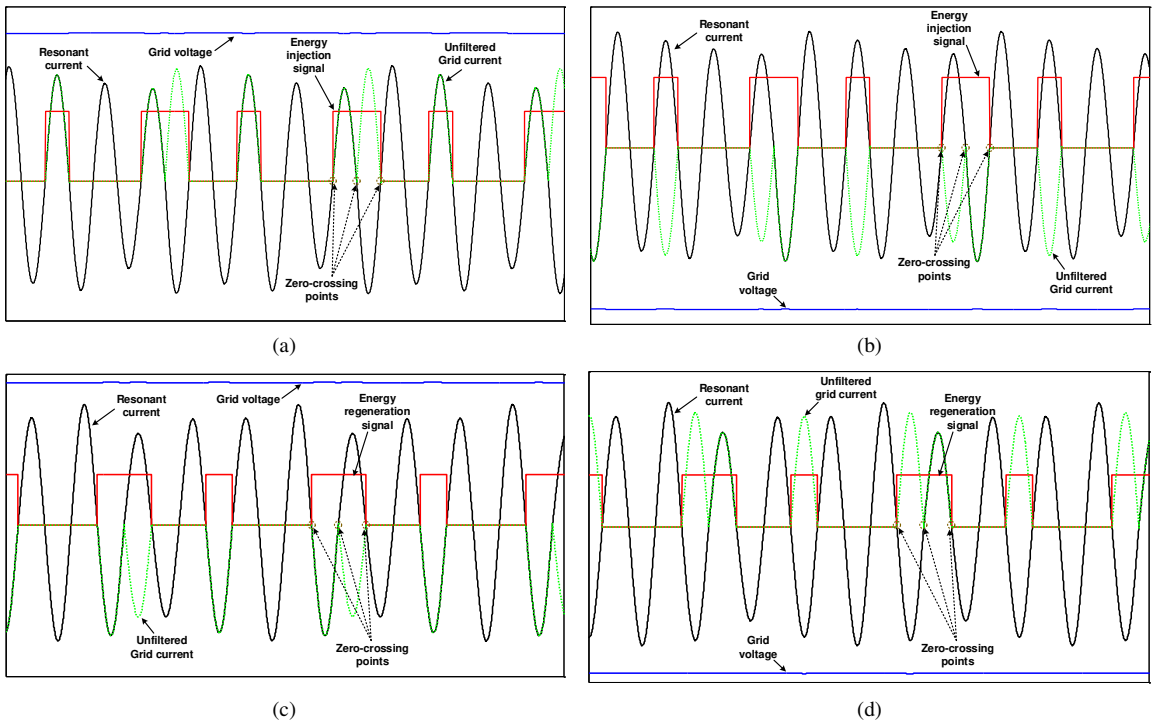

Fig. 3. Concept plot of resonant current, energy injection or regeneration signal, grid current (unfiltered) and grid voltage: (a) forward power transfer mode with positive grid voltage, (b) forward power transfer mode with negative grid voltage, (c) reverse power transfer mode with positive grid voltage, (d) reverse power transfer mode with negative grid voltage.

transfer mode, quantum energy injections increase the resonant current while in reverse power transfer mode, quantum energy regenerations decrease the resonant current.

B. Switching Logic Design

A switching logic based on the quantum energy injection/regeneration method for the single-phase AC-AC converter can be designed. This switching logic can be designed by defining different operation modes of the converter which are determined by the resonant current direction, grid voltage polarity, power transfer direction, and energy injection/regeneration signal. These operation modes are divided into three different types: energy-injection, energy-regeneration, and free-oscillation. A resonant current measurement (i_r) and an input voltage measurement (v_{ac}) are used as inputs for the switching logic. These modes are determined based on the direction of resonant current ($S_c : i_r > 0$), input voltage polarity ($S_v : v_{ac} > 0$), user-defined reverse power transfer signal ($S_r : P_g < 0$, where P_g is the grid connection power), and energy flow signal (energy injection/regeneration signal) (S_{nrg}). The S_{nrg} signal is controlled by the second section of the controller which is described in Section II-C. Zero-cross detectors with tunable hysteresis bands are employed in order to find S_c and S_v using the resonant current and grid voltage input signals. The hysteresis band can be tuned to a desired value using a positive feedback from the source signals.

The switching logic is designed in a way that in energy injection modes the output voltage of the converter and the resonant current have the same sign, and in energy regeneration modes they have opposite signs. Also, in free oscillation modes, the output voltage of the converter is zero and the resonant current is freewheeled in the LC tank. For example in an energy injection mode ($S_{nrg} = 1$, $S_r = 0$) with a positive resonant current ($i_r > 0$), a positive voltage should be applied to the IPT system and therefore, if $v_{ac} > 0$ is positive, S_{A1} and S_{B2} are turned on, and if $v_{ac} < 0$, S_{A2} and S_{B1} are turned on. In an energy regeneration mode ($S_{nrg} = 1$, $S_r = 1$) with a negative resonant current ($i_r < 0$), a positive voltage should be applied to the IPT system and therefore, if $v_{ac} > 0$ is positive, S_{A1} and S_{B2} are turned on, and if $v_{ac} < 0$, S_{A2} and S_{B1} are turned on. According to these principles, 10 operation modes can be defined in the AC-AC converter, which are presented in Table I and the corresponding resonant current paths are shown in Fig. 4. Using Table I, a switching logic can be easily obtained by expressing the switching signals S_{A1}, S_{A2}, S_{B1}, and S_{B2} as boolean equations for each switching signal in terms of S_c, S_v, S_r, and S_{nrg} as follows:

$$
\begin{aligned}
S_{A1} &= S_{nrg}\,\overline{S_r}\,(S_v\,S_c + \overline{S_v}\,\overline{S_c}) + S_{nrg}\,S_r\,(\overline{S_v}\,S_c + S_v\,\overline{S_c}) \\
S_{A2} &= S_{nrg}\,\overline{S_r}\,(\overline{S_v}\,S_c + S_v\,\overline{S_c}) + S_{nrg}\,S_r\,(S_v\,S_c + \overline{S_v}\,\overline{S_c}) \\
S_{B1} &= S_{nrg}\,\overline{S_r}\,(\overline{S_v}\,S_c + S_v\,\overline{S_c}) + \\
&\qquad S_{nrg}\,S_r\,(S_v\,S_c + \overline{S_v}\,\overline{S_c}) + \overline{S_{nrg}} \\
S_{B2} &= S_{nrg}\,\overline{S_r}\,(S_v\,S_c + \overline{S_v}\,\overline{S_c}) + \\
&\qquad S_{nrg}\,S_r\,(\overline{S_v}\,S_c + S_v\,\overline{S_c}) + \overline{S_{nrg}}
\end{aligned}
\tag{1}
$$

The direction of the power flow can be reversed by changing the S_r signal. The resonant current sign S_c which is used as a

This article has been accepted for publication in a future issue of this journal, but has not been fully edited. Content may change prior to final publication. Citation information: DOI 10.1109/TIA.2018.2820640, IEEE Transactions on Industry Applications

TABLE I
OPERATION MODES AND CORRESPONDING SWITCHING STATES OF THE SINGLE-PHASE AC-AC MATRIX CONVERTER

Mode	Type	S_r ($P_g < 0$)	S_c ($i_r > 0$)	S_v ($v_{ac} > 0$)	S_{nrg}	S_{A1}	S_{A2}	S_{B1}	S_{B2}
1	Energy injection	0	1	1	1	1	0	0	1
2	Energy injection	0	1	0	1	0	1	1	0
3	Energy injection	0	0	1	1	0	1	1	0
4	Energy injection	0	0	0	1	1	0	0	1
5	Energy regeneration	1	1	1	1	0	1	1	0
6	Energy regeneration	1	1	0	1	1	0	0	1
7	Energy regeneration	1	0	1	1	1	0	0	1
8	Energy regeneration	1	0	0	1	0	1	1	0
9	Free oscillation	–	1	–	0	0	0	1	1
10	Free oscillation	–	0	–	0	0	0	1	1

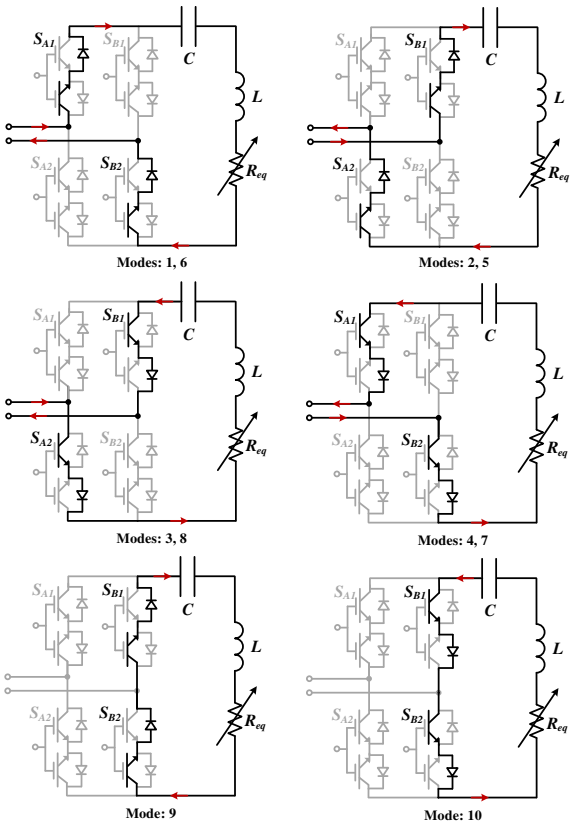

Fig. 4. Resonant current path in the single-phase AC-AC converter in 10 operation modes.

clock source for the controller is switched at resonant current zero-crossing points, based on (1) the soft-switching operations of the converter is ensured. Based on (1), a switching logic circuit is designed which is presented in Fig. 5.

In order to achieve the soft-switching operations in the converter, the transitions between operation modes are performed at zero-crossing points. This is due to the fact that the resonant current sign ($S_c : i_r > 0$) changes at each resonant current zero-crossing point. Also, the controller should be designed in such a way that any change in the energy injection/regeneration signal (S_{nrg}) occurs at resonant current zero-crossing points. Thereby, according to the boolean equations given in (1), the converter achieves zero-current switching.

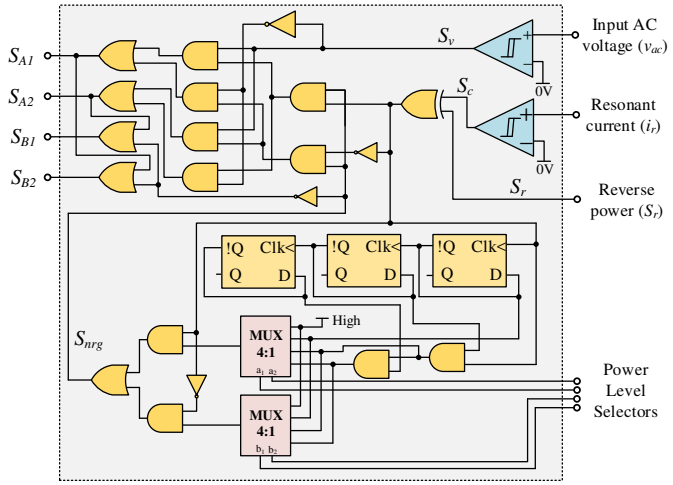

Fig. 5. The proposed power controller for the primary single-phase AC-AC converter for bidirectional IPT systems.

C. Power Transfer Controller

In an IPT system, the power transfer level can be controlled by regulating the energy transfer rate in the system. This can be achieved by controlling the number energy injection/regeneration pulses in a specific control cycle. In this study, a control cycle consisting of 8 resonant current cycles (16 half-cycles) is considered and the power transfer control is achieved by regulating the number of energy injection/regeneration half-cycles. The proposed power controller which is shown in Fig. 5, can change the number of energy injection/regeneration half-cycles to 1, 2, 4, and 8 for both positive and negative half-cycles of the resonant current. This digital controller is designed using AND, OR, NOT, XOR logic gates, flip-flops, and multiplexers. The controller generates an energy injection/regeneration signal (S_{nrg}) based on the user-defined power transfer settings (selectors) for both positive and negative resonant current half-cycles. Using the proposed power controller, 10 power transfer levels can be achieved which are presented in Table II. Each power level corresponds to a certain number of positive and negative energy injection/regeneration half-cycles, n and m, and selector state ($a_1a_2b_1b_2$).

In Fig. 3, resonant current (i_r), grid voltage (V_g), grid current (i_g), and energy injection/regeneration signal (S_{inj}/S_{reg}) in forward and reverse power transfer modes at power transfer

This article has been accepted for publication in a future issue of this journal, but has not been fully edited. Content may change prior to final publication. Citation information: DOI 10.1109/TIA.2018.2820640, IEEE Transactions on Industry Applications

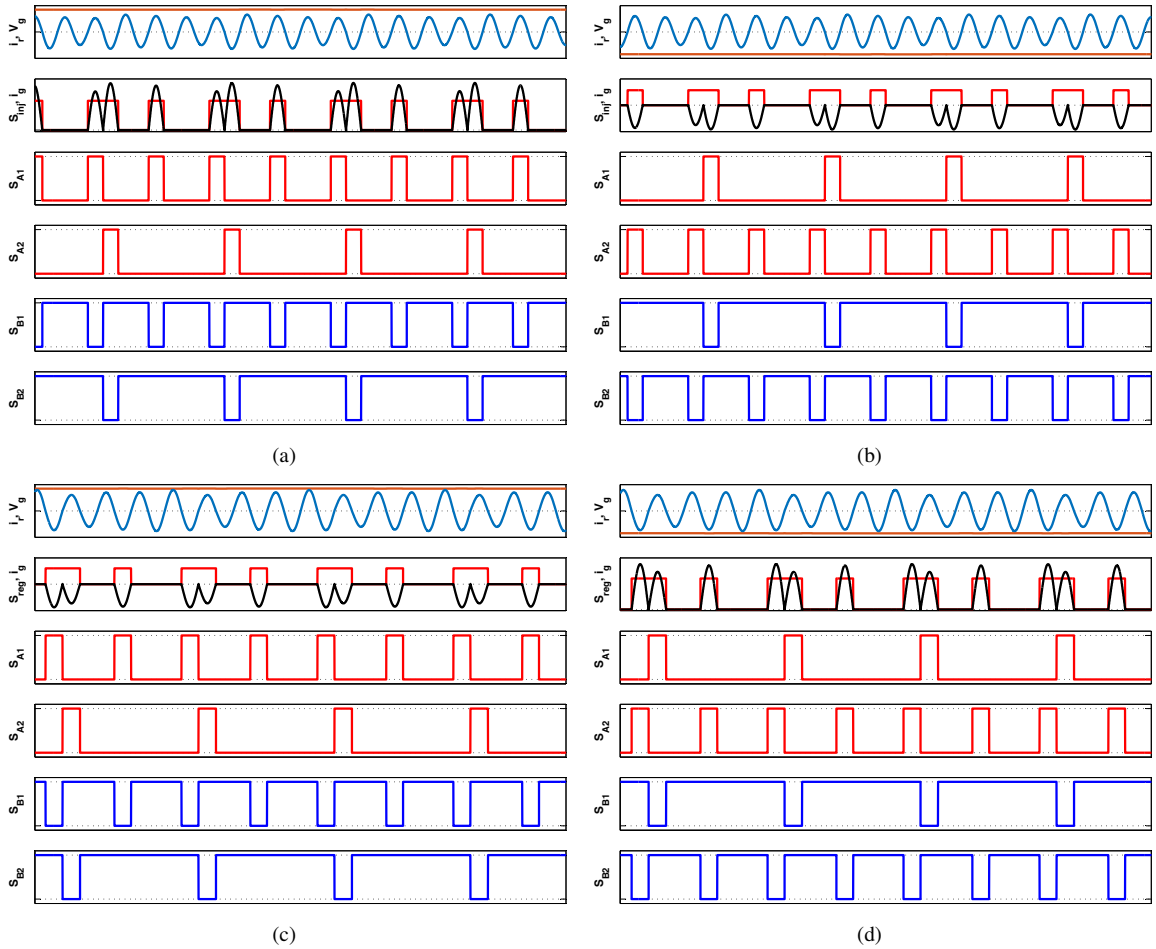

Fig. 6. Concept plot of the switching signals of the converter ($S_{A1}, S_{A2}, S_{B1}, S_{B2}$) along with the resonant current (i_r), grid voltage (V_g), energy injection/regeneration signal (S_{inj}/S_{reg}), unfiltered grid current (i_g): (a) forward power transfer mode with positive grid voltage, (b) forward power transfer mode with negative grid voltage, (c) reverse power transfer mode with positive grid voltage, (d) reverse power transfer mode with negative grid voltage.

level 6 are shown conceptually. This figure shows that using the power controller, the resonant current is rectified and directed to the single-phase grid connection in both directions. Also, the switching diagram of the converter at different operating conditions is presented as Fig. 6. This figure corresponds to the operating conditions shown in Fig. 3 and it represents the switching signals of the converter ($S_{A1}, S_{A2}, S_{B1}, S_{B2}$) along with the resonant current, grid voltage, grid current, and energy injection/regeneration signal.

D. Forward Power Transfer

The forward power transfer mode ($S_r = 0$) enables energy transfer from the primary single-phase AC source to the secondary DC source. In this case, the MC constantly switches between energy-injection and free-oscillation modes. In energy-injection modes, energy is transferred to the IPT system and as a result, the resonant current is increased. In free-oscillation modes, energy transfer to the IPT system is avoided and the resonant current is allowed to circulate in the system and the energy stored in the LC tank is used as a source for energy transfer to the IPT system. Since the energy stored in the system reduces, the resonant current decreases. Therefore, switching between these two types of modes enables power transfer regulation in forward power transfer mode. In Figs. 3(a), (b), the resonant current, energy injection signal, grid current and grid voltage are shown conceptually. It is clear that the resonant current increases in energy injection modes and it decreases in free-oscillation modes.

E. Reverse Power Transfer

The reverse power transfer mode ($S_r = 1$), is used to enable energy transfer to the primary single-phase AC source from the secondary DC source to the primary AC source. In this case, the secondary converter acts as an inverter to allow the secondary structure operate as a transmitter and in the primary MC, the energy-regeneration and free-oscillation modes are engaged. In this case, R_{eq} which represents the secondary load reflected to primary (shown in Fig. 4) is negative. This means that R_{eq} generates power (rather than consuming power) and injects power to the primary LC tank. In energy-regeneration modes, the MC transfers energy back to the primary AC source and therefore the resonant current decreases. This is done by directing the resonant current to the AC source with a

This article has been accepted for publication in a future issue of this journal, but has not been fully edited. Content may change prior to final publication. Citation information: DOI 10.1109/TIA.2018.2820640, IEEE Transactions on Industry Applications

TABLE II
POWER TRANSFER LEVELS OBTAINED USING THE POWER CONTROLLER

Power Level No.	Selector state $a_1a_2b_1b_2$	Number of energy injection/regeneration pulses		Voltage transfer ratio (G_v)
		positive pulses (m)	negative pulses (n)	
1	0000	8	8	1.0000
2	0001	8	4	0.8660
3	0010	8	2	0.7906
4	0011	8	1	0.7500
5	0101	4	4	0.7071
6	0110	4	2	0.6124
7	0111	4	1	0.5590
8	1010	2	2	0.5000
9	1011	2	1	0.4330
10	1111	1	1	0.3536

reverse polarity as shown in Fig. 3 and thereby, the energy stored in the resonant tank is injected into the grid which results in a reduction in the energy stored in the LC tank and the resonant current. Also, in free-oscillation modes, the primary current is allowed to circulate in the IPT system and thereby, energy regeneration is avoided. However, as a result of the energy transfer from the secondary to primary, in free-oscillation modes, the energy stored in the primary LC tank increases which in turn increases the resonant current. Power transfer regulation in reverse power transfer mode is enabled by continuously switching between these two types of modes.

III. THEORETICAL ANALYSIS

In this section, the power transfer rate and efficiency of the converter at different power levels are calculated theoretically and details are presented.

A. Calculation of Power Transfer

The power transfer rate of the converter at different levels can be calculated by analyzing the voltage harmonics that are generated by the converter. Since the IPT system is tuned to operate at the resonance frequency, only the harmonic components of the converter output voltage that have the resonance frequency mainly involve in the power transfer. The proposed power control method is based on a full control cycle which is composed of 8 resonant current cycles. Thus, the fundamental harmonics component at the resonance frequency can be calculated as follows:

$$V_1^{mn} = \frac{\omega}{8\pi}\int_0^{8\times\frac{2\pi}{\omega}} v_{out}\sin(\omega\, t)\, dt \tag{2}$$

where v_{out} is the instantaneous output voltage of the converter, ω is the angular resonance frequency, and V_1^{mn} is the main harmonic component of the output voltage at power level corresponding to n and m number of energy injection/regeneration pulses in positive and negative half-cycles respectively. Based on the principles of operation of the converter explained in Section II, v_{out} can be formulated as follows:

$$v_{out} = \begin{cases} \pm|v_{ac}| & \frac{2i\pi}{\omega} < t < \frac{(2i+1)\pi}{\omega},\ \frac{(2j+1)\pi}{\omega} < t < \frac{2(j+1)\pi}{\omega} \\ & i = 0, ..., m-1, \quad j = 0, ..., n-1 \\ 0 & \text{otherwise} \end{cases} \tag{3}$$

where v_{ac} is the instantaneous voltage of the single-phase AC mains. The first section of v_{out} corresponds to energy injection/regeneration modes and the second section corresponds to free-oscillation modes. The sign of the v_{out} in energy injection/regeneration modes is determined based on the power transfer mode, direction of the resonant current and the polarity of the instantaneous grid voltage. By expanding (2) using (3), the following is obtained:

$$V_1^{mn} = \frac{\pm\omega}{8\pi}\Bigg(\sum_{i=0}^{m-1}\int_{\frac{2i\pi}{\omega}}^{\frac{(2i+1)\pi}{\omega}} |v_{ac}|\sin(\omega\, t)\, dt + \sum_{i=0}^{n-1}\int_{\frac{(2i+1)\pi}{\omega}}^{\frac{2(i+1)\pi}{\omega}} |v_{ac}|\sin(\omega\, t)\, dt\Bigg) \tag{4}$$

Due to the fact that the resonance frequency is much higher than the power frequency, the variations of grid voltage in a control cycle can be neglected, and therefore (4) can be simplified as follows:

$$V_1^{mn} = \frac{\pm(m+n)|v_{ac}|}{4\pi} \tag{5}$$

It should be noted that the calculated harmonic are time variant and it is dependent on the single-phase AC mains voltage. At the resonance frequency the equivalent RLC tank is purely resistive and therefore, the fundamental harmonic of the resonant current can be calculated as follows:

$$I_1^{mn} = \frac{V_1^{mn}}{R_{eq}} = \frac{\pm(m+n)|v_{ac}|}{4\pi R_{eq}} \tag{6}$$

where R_{eq} is the equivalent resistance reflected to the primary (Fig. 4). Using (6), the power transfer rate can be obtained as:

$$P_t = \frac{1}{2}R_{eq}(I_1^{mn})^2 = \frac{(m+n)^2 v_{ac}^2}{32\pi^2 R_{eq}} \tag{7}$$

where P_t is the instantaneous power transfer rate between single-phase AC mains and IPT system. Since v_{ac} is sinusoidal, the average power transfer P_m in a full grid voltage cycle can be calculated in terms of the RMS grid voltage V_{AC} as follows:

$$P_m = \frac{(m+n)^2 V_{AC}^2}{32\pi^2 R_{eq}} \tag{8}$$

According to (8), the power controller regulates the power transfer rate by changing the number of energy injection/regeneration pulses (n and m). It should be noted that in reverse power transfer mode, R_{eq} is negative and therefore, P_m will be negative.

This article has been accepted for publication in a future issue of this journal, but has not been fully edited. Content may change prior to final publication. Citation information: DOI 10.1109/TIA.2018.2820640, IEEE Transactions on Industry Applications

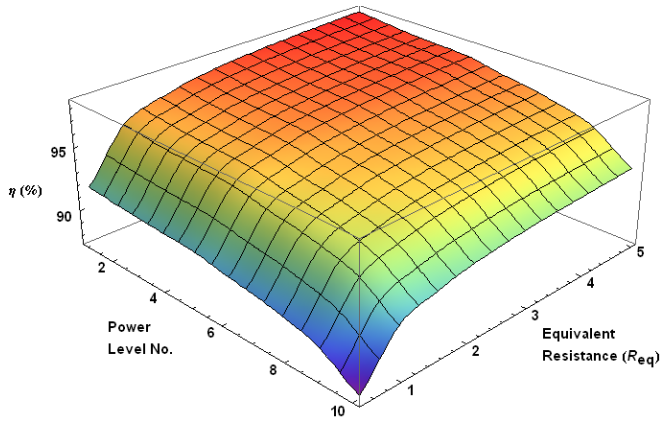

Fig. 7. The efficiency of the single-phase AC-AC converter as a function of power transfer level and equivalent reflected resistance.

B. Calculation of Voltage Transfer Ratio (VTR)

The voltage transfer ratio of the converter is defined as follows:

$$G_v = \frac{V_{out}}{V_{AC}} \tag{9}$$

where V_{out} is the RMS output voltage of the converter which can be calculated as,

$$V_{out} = \sqrt{\frac{\int_0^{2\pi/\omega_0} V_{out}^2 dt}{2\pi/\omega_0}} \tag{10}$$

where ω_0 is the angular frequency of grid voltage. It can be shown that using (3), (10) can be simplified as,

$$V_{out} = \sqrt{\frac{\frac{m+n}{16}\int_0^{2\pi/\omega_0} v_{ac}^2 dt}{2\pi/\omega_0}} \tag{11}$$

Based on the definition of V_{AC} and (11), the relation between V_{out} and V_{AC} is derived as,

$$V_{out} = \frac{\sqrt{m+n}}{4} V_{AC} \tag{12}$$

Using (9) and (12), the voltage transfer ratio (VTR) of the converter can be found as,

$$G_v = \frac{V_{out}}{V_{AC}} = \frac{\sqrt{m+n}}{4} \tag{13}$$

Equation (13) is used in order to directly calculate the voltage transfer ratio at different power transfer levels as presented in the last column of Table II.

C. Efficiency Analysis

Since the converter achieves soft-switching operations, the switching losses are negligible and its conduction losses form the major power losses of the converter. Using the proposed power controller, the switching state of the converter corresponds to one of the operation modes presented in Table I. In Fig. 4, it can be seen that in any operation mode, there are always two conducting bidirectional switches. Considering the fact that each conducting bidirectional switch is composed of one conducting power switch (MOSFET or IGBT) and one conducting body diode, the converter loss can be written as follows:

$$\begin{aligned} P_{loss} = 2(P_S + P_D) &= 2(V_{FS} I_{rms} + R_F I_{rms}^2 + V_{FD} I_{rms}) \\ &= 2\left(V_{FS} + V_{FD} + R_F I_{rms}\right) I_{rms} \end{aligned} \tag{14}$$

Using (7) and (14), the efficiency of the converter can be obtained as follows:

$$\eta = \frac{P_t}{P_t + P_{loss}} = \frac{1}{1 + \frac{R_F}{R_{eq}} + \frac{4\pi(V_{FS} + V_{FD})}{(n+m)V_{rms}}} \tag{15}$$

The efficiency of a typical AC-AC converter as a function power level number and equivalent reflected resistance which is calculated analytically using (15), is presented in Fig. 7. This figure shows that as the power level decreases, the efficiency is decreased. Also, it can be seen that the converter can achieve up to 98% efficiency.

IV. Simulation Results

A bidirectional inductive battery charging system with the proposed single-phase AC-AC MC converter as the primary converter and a conventional H-bridge converter as the secondary converter (Fig. 2) is modeled in MATLAB/Simulink. The primary converter is controlled using the proposed power controller and the secondary converter is switched using a self-tuning controller with battery charging/discharging current controller. The specifications of the case study system are presented in Table III. The simulations were carried out in 10 power transfer levels in both forward and reverse power transfer modes with 120V or 240V single-phase mains, and the results are shown in Table IV and Table V. These tables show that the proposed single-phase AC-AC converter provides a wide range of power transfer levels for both G2V and V2G connections and the IPT system can achieve power conversion efficiencies as high as 98%. In Fig. 8, the grid voltage and current, the energy injection/regeneration signals, the resonant current and the battery charging/discharging current for: (a) forward power transfer at level 2 with 120V grid voltage at the positive peak of the grid voltage, (b) forward power transfer at level 6 with 240V grid voltage at the negative peak of the grid voltage, (c) reverse power transfer at level 3 with 120V grid voltage at the positive peak of the grid voltage.

TABLE III
Specifications of the case study IPT system

Parameter	Value
Air gap	200 mm
Self-inductances (L_p, L_s)	172 μH
Compensation capacitors (C_p, C_s)	0.12 μF
Resonance frequency (f_r)	35 kHz
Grid voltage (V_{AC})	120V, 240V
Grid frequency (f_{ac})	60 Hz
Battery voltage (V_b)	360 V
Battery capacity (C_b)	22 kWh

This article has been accepted for publication in a future issue of this journal, but has not been fully edited. Content may change prior to final publication. Citation information: DOI 10.1109/TIA.2018.2820640, IEEE Transactions on Industry Applications

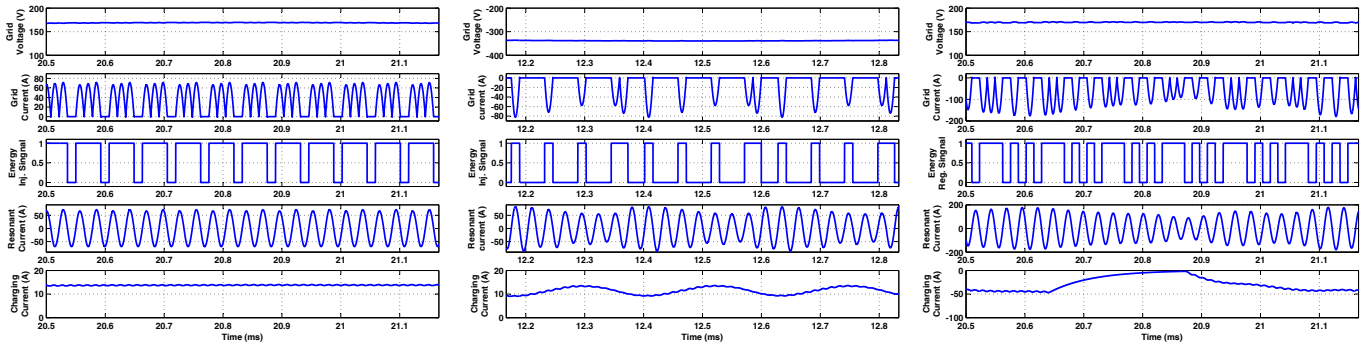

(a) (b) (c)

Fig. 8. Simulation results including the grid voltage and current, the energy injection/regeneration signals, the resonant current and the battery charging/discharging current: (a) forward power transfer at level 2 with 120V grid voltage at the positive peak of the grid voltage, (b) forward power transfer at level 6 with 240V grid voltage at the negative peak of the grid voltage, (c) reverse power transfer at level 3 with 120V grid voltage at the positive peak of the grid voltage.

TABLE IV
SIMULATION RESULTS OF THE CASE STUDY IPT SYSTEM IN FORWARD POWER TRANSFER (G2V) AT DIFFERENT POWER LEVELS

Power Transfer Level	Grid voltage (V)	Grid power (kW)	Grid current (A)	Battery current (A)	Battery power (kW)
1	120	4.77	48.52	13.18	-4.61
	240	15.52	74.16	46.8	-15.09
2	120	3.52	41.41	9.64	-3.37
	240	7.85	45.15	22.11	-7.64
3	120	2.92	37.58	7.94	-2.77
	240	6.15	39.30	17.11	-5.97
4	120	2.62	35.57	7.12	-2.48
	240	5.49	37.15	15.26	-5.31
5	120	2.32	33.37	6.26	-2.18
	240	4.78	34.37	13.20	-4.62
6	120	1.73	28.64	4.60	-1.59
	240	3.53	29.34	9.66	-3.38
7	120	1.43	25.93	3.79	-1.30
	240	2.93	26.70	8.04	-2.78
8	120	1.14	22.95	2.94	-1.01
	240	2.33	23.69	6.28	-2.18
9	120	0.84	19.55	2.13	-0.72
	240	1.73	20.23	4.67	-1.59
10	120	0.54	15.48	1.28	-0.43
	240	1.14	16.21	2.95	-1.01

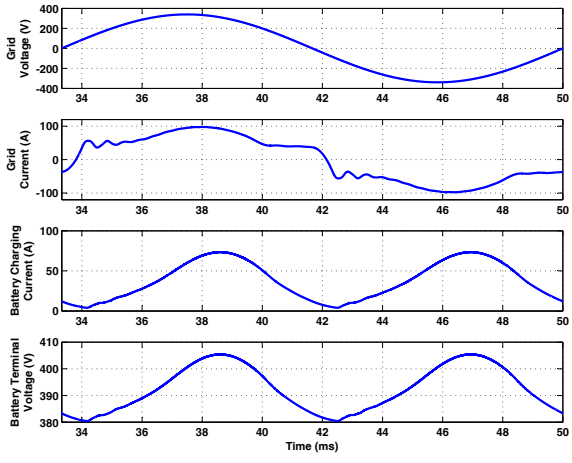

Fig. 9. The simulation results of a G2V connection at the maximum power transfer level (15 kW) in a full grid voltage cycle showing grid voltage, grid current, battery charging voltage and current.

TABLE V
SIMULATION RESULTS OF THE CASE STUDY IPT SYSTEM IN REVERSE POWER TRANSFER (V2G) AT DIFFERENT POWER LEVELS

Power Transfer Level	Grid voltage (V)	Grid power (kW)	Grid current (A)	Battery current (A)	Battery power (kW)
1	120	-9.76	100.16	31.73	10.60
	240	-13.28	76.94	38.81	13.87
2	120	-7.19	85.45	26.08	8.01
	240	-10.95	73.10	33.13	11.60
3	120	-6.04	78.99	23.62	6.92
	240	-9.82	69.76	30.37	10.53
4	120	-5.44	74.81	22.30	6.30
	240	-9.16	68.08	29.24	9.85
5	120	-4.80	69.78	20.49	5.64
	240	-9.75	70.89	31.87	10.63
6	120	-3.64	61.46	17.77	4.46
	240	-7.16	60.78	26.01	8.00
7	120	-3.04	56.32	16.38	3.99
	240	-5.99	56.12	23.55	6.82
8	120	-2.47	50.89	15.35	3.49
	240	-4.79	49.64	20.47	5.63
9	120	-1.86	44.10	13.49	2.83
	240	-3.62	43.41	17.78	4.48
10	120	-1.19	34.77	10.27	2.08
	240	-2.43	35.56	14.87	3.42

As it can be seen, since the resonance frequency of the IPT system is much higher than the frequency of the single-phase mains, the variations of the grid voltage in a few cycles of the resonant current is negligible and the grid voltage can be assumed to be constant. Figs. 8(a) and (b) show that in G2V connections, the grid current and voltage are of the same sign and the battery charging current is positive which confirm that the power that is being transferred to the battery is positive. Also, the figures show that free-oscillation modes cause a reduction in the energy stored in the IPT system and thereby reduce the resonant current. Conversely, Figs. 8(c) and (d) show that in V2G connections, the grid current and voltage have an opposite sign and the battery charging current is negative, which confirms that the power is being transferred to the grid is positive. Similarly, the figures show that free-oscillation modes cause an increase in the energy stored in the IPT system and thereby increase the resonant current. Moreover, the grid current is determined by the energy

This article has been accepted for publication in a future issue of this journal, but has not been fully edited. Content may change prior to final publication. Citation information: DOI 10.1109/TIA.2018.2820640, IEEE Transactions on Industry Applications

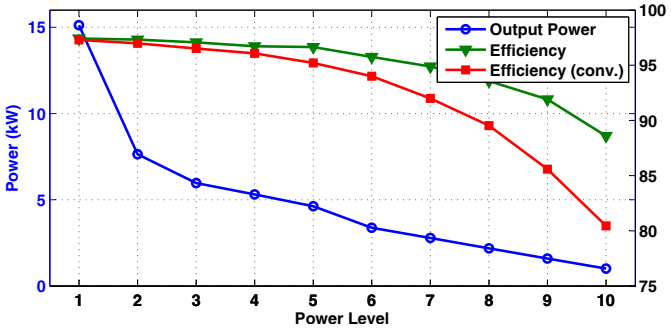

Fig. 10. The efficiency of a single-phase AC-AC converter controlled using the proposed power controller and conventional controller at different power transfer levels calculated based on simulations.

engagement signal (S_{nrg}) and when $S_{nrg} = 0$ it is zero and when $S_{nrg} = 1$, it equals to the rectified resonant current (i_r).

In Fig 9, the simulation results of a forward power transfer mode at the maximum power level (15 kW) in a full grid voltage cycle showing grid voltage, grid current, battery charging voltage and current are presented. This figure shows that the grid voltage variations lead to variations in battery charging current. Moreover, it can be seen that the LC filter has significantly reduced the harmonics associated with energy injection/regeneration current pulses of the primary side. Calculations show that the grid current has a Total Harmonic Distortion (THD) of 19%. It should be noted that the grid current THD still can be improved more by using higher order power filters.

In Fig. 10, the efficiency calculations based on both the proposed power controller and a conventional controller at different power transfer levels are presented. The conventional power controller is simulated based on the firing angle control method with respect to zero-current crossing points to regulate the power transfer rate. The results show that in both cases the converter can reach efficiencies as high as 98% at the maximum power level (Level 1). As the power level decreases, the proposed converter significantly outperforms the conventional controller and at power level 10 it can achieve 8% higher efficiency. This is mainly due to the fact that the proposed power controller ensures soft-switching operations of the converter at all power transfer level.

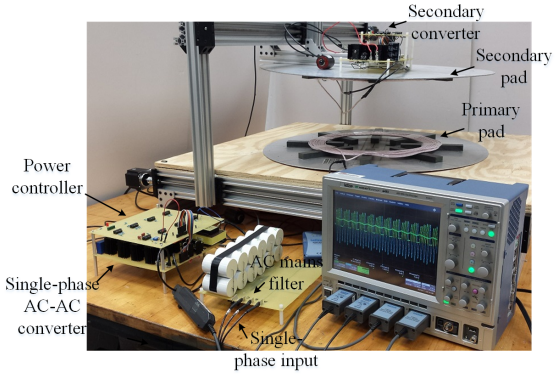

Fig. 11. The IPT system setup comprised of primary and secondary pads, primary AC-AC matrix converter controlled using the proposed power transfer controller, and the secondary converter.

TABLE VI
SPECIFICATIONS OF THE CASE STUDY IPT SYSTEM SETUP

Parameter	Components	Value
Pad self-inductance	15 turns, 10 AWG Litz wire	172 μH
Compensation capacitors	Film capacitor, FPG66Y0124J	120 nF
Primary supply	Variable three-phase AC supply	20 V (LL), 60 Hz
Secondary battery	Lead-acid battery	12 V, 86.4 Wh

V. EXPERIMENTAL RESULTS

The proposed single-phase AC-AC converter and its power controller are built and experimental tests were carried out on a case study IPT system which is shown in Fig. 11. The IPT system setup includes series compensated transmitter and receiver power pads with 200mm air gap, primary AC-AC converter, secondary H-bridge converter. The power controller of the primary AC-AC converter is built according to the circuit presented in Fig. 5. A variable single-phase AC supply is used as a grid connection. The details of the IPT system setup specifications are presented in Table VI. An LC power filter is used on the primary side for mitigation of the harmonics generated by the proposed single-phase AC-AC converter. This filter is designed to have a cut-off frequency less than one-sixth of the switching frequency of the converter (resonance frequency). The LC filter is composed of L=40μH, C=20μF with a cut-off frequency of 5.6 kHz.

The experimental results including the grid voltage and current (unfiltered), the energy injection/regeneration signals, and the resonant current are shown in Fig. 12. Figures 12(a), (b), (c) and (d) show forward power transfer at levels 2 and 3 at positive and negative peak grid voltage. Figures 12(e), (f), (g) and (h) show reverse power transfer at levels 6 and 7 at positive and negative peak grid voltage. These figures show that the AC-AC converter can effectively establish single-phase G2V and V2G connections at different power transfer levels with resonance frequency tracking capability and soft-switching operations.

As it is shown in Fig. 12, in forward power transfer modes, the grid current and voltage have same signs and therefore, the power is being transferred from the primary AC supply to the secondary. In reverse power transfer modes, the grid current and voltage have opposite signs and thus, the power is being transferred from the secondary to the primary AC supply. The power controller is designed to allow the resonant current to continue its damped oscillation regardless of power transfer level and direction of power. This enables the resonance frequency tracking capability and ensures high power transfer efficiency as the converter operates at the damped resonance frequency of the IPT system (frequency of resonant current). The transitions to different operation modes occur at the resonant current zero-crossing points which enable soft-switching operations. The grid voltage has small variations that are due to the energy injection/regeneration to/from the IPT system. The efficiency measurements at 95W show that the single-phase AC-AC converter can achieve 92% efficiency at level 1 in both forward and reverse power transfer modes.

This article has been accepted for publication in a future issue of this journal, but has not been fully edited. Content may change prior to final publication. Citation information: DOI 10.1109/TIA.2018.2820640, IEEE Transactions on Industry Applications

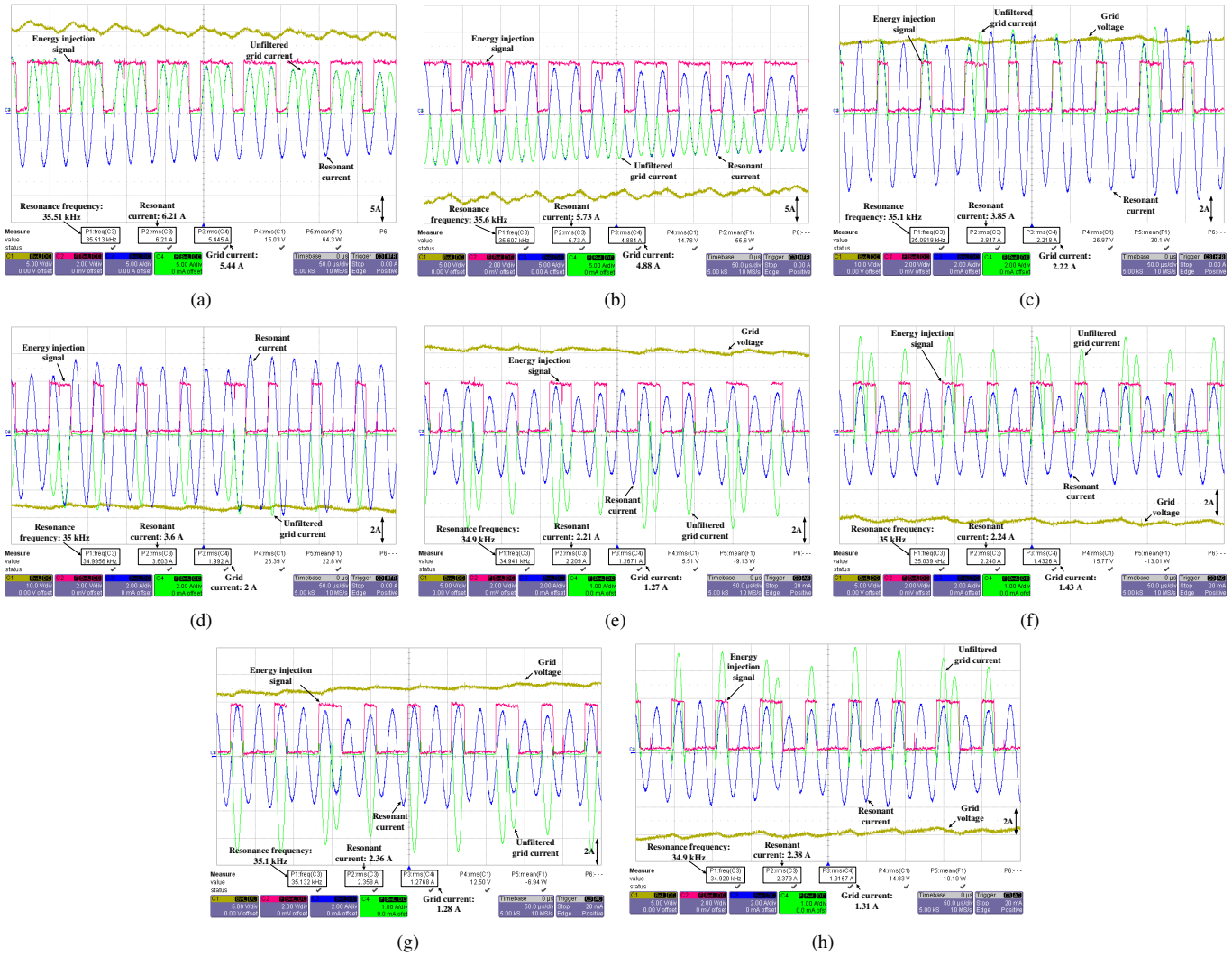

Fig. 12. Experimental test results on the case study IPT system setup including the grid voltage and current (unfiltered), the energy injection/regeneration signals, and the resonant current: (a), (b) level 2 forward power transfer at positive and negative peak grid voltage, (c), (d) level 6 forward power transfer at positive and negative peak grid voltage, (e), (f) level 6 reverse power transfer at positive and negative peak grid voltage, (g), (h) level 7 reverse power transfer at positive and negative peak grid voltage.

The efficiency of the converter significantly increases as the power level increase and as it is shown in Fig. 10, it can achieve efficiencies as high as 98%.

VI. Conclusion

The proposed direct single-phase AC-AC converter along with the proposed power transfer controller can be used as an alternative to conventional two-stage converters for bidirectional IPT systems. Due to the elimination of AC-DC conversion stage and bulky DC-link capacitors, the converter is more compact and reliable compared to conventional two-stage converters. The power transfer controller which is designed based on the energy injection/regeneration principle and is implemented based on simplified logic design, effectively enables bidirectional power transfer at 10 different power levels. The resonance frequency tracking capability ensures that the converter operates exactly at the damped resonance frequency of the IPT system and therefore, power transfer efficiency with high efficiency can be achieved. Also, the converter benefits from soft-switching operations that further enhances the efficiency of the converter. Finally, the structure of the single-phase matrix converter along with the simplified controller makes it suitable for residential inductive charging systems with bidirectional power flow capability. The resonance frequency tracking capability of the converter makes it suitable for inductive EV charging systems, in which the system may have variations. The bidirectional power transfer capability can be used to make single-phase G2V and V2G connections through IPT systems at multiple power levels including those defined by SAE J2954 standard.

References

[1] C.-S. Wang, O. H. Stielau, and G. A. Covic, "Design considerations for a contactless electric vehicle battery charger," *IEEE Trans. Ind. Electron.*, vol. 52, no. 5, pp. 1308–1314, Oct 2005.

[2] J. M. Miller and A. Daga, "Elements of wireless power transfer essential to high power charging of heavy duty vehicles," *IEEE Trans. Transport. Electrific.*, vol. 1, no. 1, pp. 26–39, June 2015.

[3] M. Budhia, G. Covic, and J. Boys, "Design and optimization of circular magnetic structures for lumped inductive power transfer systems," *IEEE Trans. Power Electron.*, vol. 26, no. 11, pp. 3096–3108, Nov 2011.

[4] G. Buja, C. T. Rim, and C. C. Mi, "Dynamic charging of electric vehicles by wireless power transfer," *IEEE Trans. Ind. Electron.*, vol. 63, no. 10, pp. 6530–6532, Oct 2016.

[5] G. Buja, M. Bertoluzzo, and H. K. Dashora, "Lumped track layout design for dynamic wireless charging of electric vehicles," *IEEE Trans. Ind. Electron.*, vol. 63, no. 10, pp. 6631–6640, Oct 2016.

[6] C. C. Mi, G. Buja, S. Y. Choi, and C. T. Rim, "Modern advances in wireless power transfer systems for roadway powered electric vehicles," *IEEE Trans. Ind. Electron.*, vol. 63, no. 10, pp. 6533–6545, Oct 2016.

[7] T. V. Theodoropoulos, I. G. Damousis, and A. J. Amditis, "Demand-side management ict for dynamic wireless ev charging," *IEEE Trans. Ind. Electron.*, vol. 63, no. 10, pp. 6623–6630, Oct 2016.

[8] J. H. Kim, B. S. Lee, J. H. Lee, S. H. Lee, C. B. Park, S. M. Jung, S. G. Lee, K. P. Yi, and J. Baek, "Development of 1-mw inductive power transfer system for a high-speed train," *IEEE Trans. Ind. Electron.*, vol. 62, no. 10, pp. 6242–6250, Oct 2015.

[9] B. X. Nguyen, D. M. Vilathgamuwa, G. H. B. Foo, P. Wang, A. Ong, U. K. Madawala, and T. D. Nguyen, "An efficiency optimization scheme for bidirectional inductive power transfer systems," *IEEE Trans. Power Electron.*, vol. 30, no. 11, pp. 6310–6319, Nov 2015.

[10] J. Y. Lee and B. M. Han, "A bidirectional wireless power transfer ev charger using self-resonant pwm," *IEEE Trans. Power Electron.*, vol. 30, no. 4, pp. 1784–1787, April 2015.

[11] M. J. Neath, A. K. Swain, U. K. Madawala, and D. J. Thrimawithana, "An optimal pid controller for a bidirectional inductive power transfer system using multiobjective genetic algorithm," *IEEE Trans. Power Electron.*, vol. 29, no. 3, pp. 1523–1531, March 2014.

[12] U. K. Madawala and D. J. Thrimawithana, "A bidirectional inductive power interface for electric vehicles in v2g systems," *IEEE Trans. Ind. Electron.*, vol. 58, no. 10, pp. 4789–4796, Oct 2011.

[13] M. J. E. Alam, K. M. Muttaqi, and D. Sutanto, "A controllable local peak-shaving strategy for effective utilization of pev battery capacity for distribution network support," *IEEE Trans. Ind. Appl.*, vol. 51, no. 3, pp. 2030–2037, May 2015.

[14] J. A. Suul, S. D'Arco, and G. Guidi, "Virtual synchronous machine-based control of a single-phase bi-directional battery charger for providing vehicle-to-grid services," *IEEE Trans. Ind. Appl.*, vol. 52, no. 4, pp. 3234–3244, July 2016.

[15] A. Namadmalan, "Bidirectional current-fed resonant inverter for contactless energy transfer systems," *IEEE Trans. Ind. Electron.*, vol. 62, no. 1, pp. 238–245, Jan 2015.

[16] U. K. Madawala, M. Neath, and D. J. Thrimawithana, "A power-frequency controller for bidirectional inductive power transfer systems," *IEEE Trans. Ind. Electron.*, vol. 60, no. 1, pp. 310–317, Jan 2013.

[17] N. S. Gonzlez-Santini, H. Zeng, Y. Yu, and F. Z. Peng, "Z-source resonant converter with power factor correction for wireless power transfer applications," *IEEE Trans. Power Electron.*, vol. 31, no. 11, pp. 7691–7700, Nov 2016.

[18] J. I. Rodriguez and S. B. Leeb, "A multilevel inverter topology for inductively coupled power transfer," *IEEE Trans. Power Electron.*, vol. 21, no. 6, pp. 1607–1617, Nov 2006.

[19] S. Weerasinghe, U. K. Madawala, and D. J. Thrimawithana, "A matrix converter-based bidirectional contactless grid interface," *IEEE Trans. Power Electron.*, vol. 32, no. 3, pp. 1755–1766, March 2017.

[20] H. L. Li, A. P. Hu, and G. A. Covic, "A direct ac-ac converter for inductive power-transfer systems," *IEEE Trans. Power Electron.*, vol. 27, no. 2, pp. 661–668, Feb 2012.

[21] M. Moghaddami, A. Anzalchi, and A. I. Sarwat, "Single-stage three-phase ac-ac matrix converter for inductive power transfer systems," *IEEE Trans. Ind. Electron.*, vol. 63, no. 10, pp. 6613–6622, Oct 2016.

[22] L. G. G. de Vicuna, M. Castilla, J. Miret, J. Matas, and J. M. Guerrero, "Sliding-mode control for a single-phase ac/ac quantum resonant converter," *IEEE Trans. Ind. Electron.*, vol. 56, no. 9, pp. 3496–3504, Sept 2009.

[25] A. Namadmalan, "Self-oscillating tuning loops for series resonant inductive power transfer systems," *IEEE Trans. Power Electron.*, vol. 31, no. 10, pp. 7320–7327, Oct 2016.

[23] C. T. Rim and G. H. Cho, "Quantum transformation: the analysis of quantum rectifier-inverters," in *Conference Record of the IEEE Industry Applications Society Annual Meeting,*, Oct 1989, pp. 1081–1085 vol.1.

[24] M. Moghaddami and A. Sarwat, "Self-tuning variable frequency controller for inductive electric vehicle charging with multiple power levels," *IEEE Trans. Transport. Electrific.*, vol. 3, no. 2, pp. 488–495, June 2017.

[26] M. Moghaddami, A. Sundararajan, and A. I. Sarwat, "A power-frequency controller with resonance frequency tracking capability for inductive power transfer systems," *IEEE Trans. Ind. Appl.*, vol. 54, no. 2, pp. 1773–1783, March 2018.

[27] M. Moghaddami, A. Cavada, and A. I. Sarwat, "Soft-switching self-tuning h-bridge converter for inductive power transfer systems," in *2017 IEEE Energy Conversion Congress and Exposition (ECCE)*, Oct 2017, pp. 4388–4392.

[28] M. Moghaddami and A. Sarwat, "Self-tuned single-phase ac-ac converter for bidirectional inductive power transfer systems," in *2017 IEEE Industry Applications Society Annual Meeting*, Oct 2017, pp. 1–6.

[29] SAE International, "J2954," *Wireless Power Transfer for Light-Duty Plug-In/Electric Vehicles and Alignment Methodology*, 2016.

Masood Moghaddami (S'15) received the B.S. degree from the Amirkabir University of Technology, Tehran, Iran, in 2009, and the M.S. degree from the Iran University of Science and Technology, Tehran, in 2012, both in electrical engineering.

From 2011 to 2014, he worked in industry as an application engineer on the design optimization of large power transformers, power stabilizers and automatic voltage regulators. He is currently working toward the Ph.D. degree in electrical engineering with the Department of Electrical and Computer Engineering, Florida International University, Miami, FL, USA. His research interests include power electronics, digital control, and renewable energy systems, and electromagnetics.

Arif I. Sarwat (M'08-SM'16) received the master's degree from the University of Florida, Gainesville, FL, USA, in 2005, and the Ph.D. degree from the University of South Florida, Tampa, FL, in 2010, both in electrical engineering.

He is currently an Associate Professor and the Director with the Solar Research Facility,Department of Electrical and Computer Engineering, Florida International University (FIU), Miami, FL, where he leads the Energy Power and Sustainability Group. His research interests include smart grids, plug-in hybrid and electric vehicle (PHEV and EV) systems, high-penetration renewable systems, grid resiliency, large-scale data analysis, advanced metering infrastructure, smart city infrastructure, and cyber security.

Dr. Sarwat was the recipient of the National Science Foundation CAREER Award in 2016, and the recipient of multiple federal and industry research awards. He was the author/co-author of conference best paper awards from the Resilience Week in 2017 and a Journal Best Paper Award in 2016 from Modern Power Systems and Clean Energy. He was also the recipient of the Faculty Award for Excellence in Research and Creative Activities in 2016, the College of Engineering and Computing Worlds Ahead Performance in 2016, and the FIU Top Scholar Award in 2015. He won three recognition awards from Siemens. He is the Chair of IEEE Miami Section Vehicular Technology and Communication since 2012.